ADVANCED OPTICAL MATERIALS

www.advopticalmat.de

Fano Resonance in Artificial Photonic Molecules

Guangtao Cao, Shaohua Dong, Lei-Ming Zhou, Qing Zhang, Yan Deng, Cong Wang, Han Zhang, Yang Chen, Cheng-Wei Qiu, and Xinke Liu**

The spectral signatures of chemical molecules are dependent on the hybridization of electronic states. The artificial photonic molecules formed by structured optical microcavities, exhibiting Fano features with sharp asymmetric line shape and strong field enhancement, hold various potential applications in sensors, optical switches, lasing spasers, optical diodes, etc. To design high-performance photonic devices, it is of great importance to gain the formation and modulation mechanisms of Fano resonance in various artificial photonic molecules. This review is focused on the Fano resonance in artificial photonic molecules. It starts by discussing the properties of Fano resonance, followed by a detailed discussion of the coupled oscillator model and coupled mode theory that could reveal the underlying mechanisms. Then, different types of photonic molecules for realizing Fano resonance are presented, and several representative exciting applications are introduced. Finally, a summary and a brief outlook on challenges are discussed for Fano resonance in artificial photonic molecules.

1. Introduction

Fano resonance, a fundamentally interesting feature resulting from the interference between a discrete narrow localized state and the background broadband continuum, exhibits an asymmetric line shape with a high quality factor, which can sustain significantly enhanced modal fields,[1–5] and enable numerous photonic applications, such as optical switching,[6–9] sensing,[10–15] nonreciprocal propagation,[16–21] modulation,[22–26] optical logic gates,[27–29] and light buffering and storage.[3,30–35]

The Fano line shape profiles are related to the system's structural parameters and the electromagnetic parameters of ambient media. So, various systems, including optical cavities,[36–39] nanoclusters,[40–43] photonic crystals,[44–45] gratings,[46–49] metamaterials,[50–53] metasurfaces,[54–57] and many others,[58–63] have been proposed theoretically and observed experimentally to exhibit Fano resonance. Inspired by recent progress in numerous novel materials,[64–69] including 2D materials with exotic optoelectronic properties,[70–72] superconducting materials,[73,74] phase-changed materials,[75,76] low loss dielectric materials[77,78] and quantum dots,[79–82] many opportunities to investigate Fano resonance are anticipated.

It is well-known that the macroscopically arrayed structures are typically too bulky for highly integrated on-chip optical circuits, thus, compact photonic structures are in high demand.[83–85] Optical microcavities, with high quality (high-Q) factors, convenient all-optical control, and compatibility with on-chip fabrication, have been used extensively for sophisticated optical devices, such as isolators,[86] lasers,[87] circuits,[88] sensors,[89–91] and buffers,[92,93] with distinctive properties. Based on the similarities between the classical electromagnetism and quantum mechanics, a single cavity and coupled-cavity can be referred to as artificial photonic atom and photonic molecule,[94–96] respectively. Analogous to the single atom molecule, a single cavity can also be referred to as a photonic molecule. The spectral response arising from the coherent interaction of optical modes depends heavily on the configuration of the artificial photonic molecules.[97–99]

Over the years, sorts of photonic molecules have been implemented as key building blocks for realizing Fano resonance,[83,85,88–91,100,101] thanks to the interactions between optical modes as illustrated in **Figure 1**a. The Fano profiles have been both experimentally and theoretically studied with numerous interesting physical phenomena revealed by the coupled oscillator model,[83,86,102] temporal coupled-mode theory,[103–107] transfer matrix method,[108–110] and quantum-optics approach.[111,112] In this work, we focus on reviewing the Fano resonance in artificial photonic molecules. We first introduce the properties of Fano resonance. Specifically, we discuss

Dr. G. Cao, Prof. X. K. Liu
College of Materials Science and Engineering
Shenzhen University
Shenzhen 518060, China
E-mail: xkliu@szu.edu.cn

Dr. G. Cao, Dr. S. Dong, Dr. L.-M. Zhou, Dr. Q. Zhang, Dr. Y. Deng, Dr. Y. Chen, Prof. C.-W. Qiu
Department of Electrical and Computer Engineering
National University of Singapore
Kent Ridge, Singapore 117583, Singapore
E-mail: chengwei.qiu@nus.edu.sg

Dr. S. Dong, Dr. C. Wang, Prof. H. Zhang
Collaborative Innovation Center for Optoelectronic Science and Technology
International Collaborative Laboratory of 2D Materials for Optoelectronics Science and Technology of Ministry of Education
College of Optoelectronic Engineering
Shenzhen University
Shenzhen 518060, China

The ORCID identification number(s) for the author(s) of this article can be found under https://doi.org/10.1002/adom.201902153.

DOI: 10.1002/adom.201902153

the coupled oscillator model and coupled mode theory for Fano features, followed by the realization of Fano resonance in various stereotypical photonic molecules. Next, the applications of Fano resonance in photonic molecules are reviewed, including optical switching, optical sensing, and nonreciprocal propagation. Finally, the challenges and future outlooks are discussed.

2. Properties of Fano Resonance

The Fano resonance was discovered in 1935, when Beutler observed an asymmetric line shape in the absorption spectra of noble gasses, which at that time could not be accounted for by the Lorentzian model.[113] Later, Ugo Fano established the first theoretical explanation for the phenomena.[1] In his formula, the asymmetric line shape originates from the interference between discrete states and continuum states.[83,85,86,90,114–118] The Fano profile, different from the symmetric Lorentzian profile, can be described by the following equation[2,83–86]

$$F(\lambda) = F_0 \frac{(q+\delta)^2}{1+\delta^2} + A_0 \tag{1}$$

where the normalized frequency detuning $\delta = 2(\omega - \omega_0)/\Gamma$, ω is the frequency of the incident light, ω_0 is the resonance frequency, Γ is the narrow resonance bandwidth, F_0 denotes the amplitude of the Fano resonance, A_0 is the background component, c is the velocity of light in vacuum, and q is the Fano parameter, which is the ratio between the resonant state and nonresonant state. As shown in Figure 1b, $|q| \to \infty$ and $q = 0$ correspond to Lorentzian line shape and quasi-Lorentzian line shape, respectively. For $|q| \to \infty$ ($q = 0$), the maximum (minimum) of the normalized Fano line shape is located at the resonant frequency. The case $q = 1$ indicates that the Fano peak is located at a higher frequency than the dip, while the case $q = -1$ indicates that the peak is located at a lower frequency than the Fano dip. For the cases of $q = 1$ and $q = -1$, both the resonance frequencies are in the middle of the maximum and minimum of the Fano line shape.

Figure 1c shows a three-level atomic system, where $|1\rangle$, $|2\rangle$, and $|3\rangle$ correspond to the ground state, metastable state and excited state, respectively.[87] Due to the probe field and control field, the ground state and metastable state couple to the excited state, thus the transitions $|1\rangle \to |3\rangle$ and $|2\rangle \to |3\rangle$ are allowed while the transition $|1\rangle \to |2\rangle$ is forbidden. To realize an atom in the excited state, there are the direct transition path $|1\rangle \to |3\rangle$ and indirect transition path $|1\rangle \to |3\rangle \to |2\rangle \to |3\rangle$. When the decay rate of the metastable state $|2\rangle$ is small and the probe field is much weaker than the control field, the transition probability amplitude of the indirect path is comparable to that of the direct path. For a detuned field, the direct path and indirect path do not have a π phase shift, which gives rise to the Fano type transmission spectra for probe field. For the resonant field, both the transitions from $|2\rangle$ to $|3\rangle$ and $|3\rangle$ to $|2\rangle$ introduce a $\pi/2$ phase shift, so the phase shift between the direct path and indirect path is equal to π, and the transitions cancel.[1,114]

When a strong control field is applied to the transition between the metastable state $|2\rangle$ and excited state $|3\rangle$, which leads to two dressed states $|\pm\rangle = (|3\rangle \pm |2\rangle)/\sqrt{2}$, arising from the splitting of the excited state $|3\rangle$. An atom in the ground state can be excited to the two dressed states. As the probe field enables the transition from $|1\rangle$ to $|3\rangle$, the opposite contributions arising from the two dressed states give rise to the electromagnetically induced transparency/Fano phenomena.[114] Under certain conditions, Fano-type line shape evolves into an electromagnetically induced transparency (EIT) line shape profile, and EIT can be viewed as a particular case of Fano resonance.[83,86,111,112]

Guangtao Cao received his Ph.D. degree from the Central South University, Changsha, Hunan, China. He is a visiting fellow of National University of Singapore, and also working as a postdoctor with Shenzhen University, China. His research interests include the surface plasmons, plasmonic waveguide, optical microcavity, optical sensing, optical confinement, and optical focusing.

Cheng-Wei Qiu received his B.Eng. and Ph.D. degrees in 2003 and 2008, respectively. After a postdoc at Massachusetts Institute of Technology, USA, he joined National University of Singapore (NUS) as an assistant professor in 2009 and was promoted to associate professor with tenure in 2017. In January 2018, he was promoted to dean's chair in the Faculty of Engineering, NUS. His current research interests include silicon nanophotonics, optomechanics, Fano resonance in silicon, and metasurfaces.

Xinke Liu received his B. Appl. Sc. (Hons) degree (2008) in Materials Science and Ph.D. degree (2013) in Electrical and Computer Engineering from National University of Singapore. He has authored or co-authored more than 100 journal and conference papers, and his research is related to 2D and GaN-based electronic and photonic devices. He is currently an assistant professor/research professor with Shenzhen University, China.

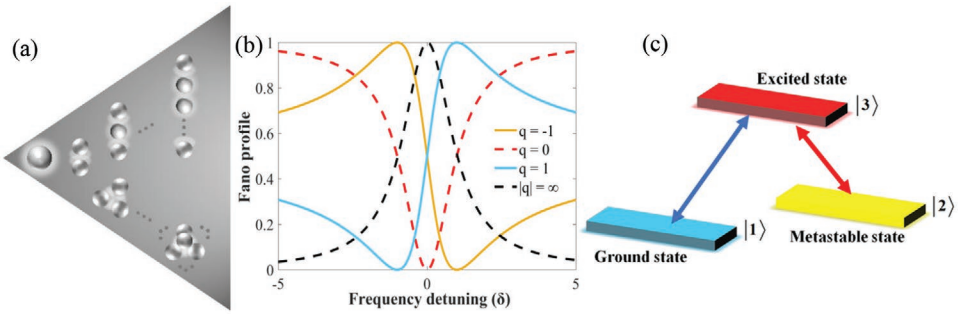

Figure 1. Schematic of photonic molecule geometries and energy levels in an atomic system for Fano resonance. a) Illustration of photonic molecules for Fano resonance. Top: each cavity in a photonic molecule only interacts with adjacent cavities. Bottom: each cavity in the photonic molecules can interact with all other cavities directly. b) Normalized Fano profiles versus various values of the Fano parameter q. c) A three-level atomic system.

3. Theoretical Model for Fano Resonance

The realization of Fano resonance in classical systems has been investigated theoretically and experimentally. To better understand the physics of Fano resonance, a great number of publications have proposed different theoretical models to reveal the origin of Fano resonance in a variety of nanoscale structures. The coupled oscillator model and coupled mode theory have been frequently used in the context of photonic molecules to interpret the significant features.[2,44,83,103] Thus, in this section, we will mainly discuss these two theoretical models to visualize the optical mode interactions in selected structured photonic molecules.

3.1. Coupled Oscillator Model

In many cases, a resonance can be described as a harmonic oscillator with a driving force.[2] For suitably designed photonic molecules composed of optical microcavities, the Fano phenomena can be theoretically explained using the coupled oscillator model.[2,83,44,119–122]

For multiple coupled oscillators, as shown in **Figure 2**a, each oscillator is driven by forces with identical magnitude $f(t) = f(\omega)\exp(-i\omega t)$ with the driving frequency ω.[122] Assuming the excitation of the lth resonator $p_l(t) = p_l(\omega)\exp(-i\omega t)$ (l = 1,2... N), the coupled harmonic matrix equation in the frequency domain can be described as

$$D_j p_j(\omega) + \sum_{l=1, l\neq j}^{N} \kappa_{jl} p_l(\omega) = f(\omega) \tag{2}$$

where $D_j = 1 - (\omega/\omega_j)^2 - i\gamma_j(\omega/\omega_j)$ (j = 1, 2,..., N), κ_{jl} (j = 1, 2,..., N, l = 1, 2,..., N, $\kappa_{lj} = \kappa_{jl}$, $l \neq j$) denotes the coupling coefficient between the jth resonator and lth resonator, and $p_l(\omega)$, ω_l and γ_l are the excitation, angular resonance frequency, and damping factor of the lth resonator, respectively. In the multiple coupled oscillators model, the surface conductivity $\sigma_N = -i\omega\sum\theta_j p_j(\omega)/f(\omega)$ is used to describe the spectral response, where θ_j denotes the weighting coefficient of the excitation $p_j(\omega)$. After solving Equation (2), the power transmission and reflection of the classical system can be expressed as

$$T = \left|\frac{2}{2+\zeta\sigma_N}\right|^2, R = \left|\frac{\zeta\sigma_N}{2+\zeta\sigma_N}\right|^2 \tag{3}$$

where ζ denotes the wave impedance of external waves, and is strongly dependent on the system parameters.[119,122] It is apparent that, in Equations (2) and (3), both the wave impedance ζ and surface conductivity σ_N are critical to controlling the Fano resonance line shape. In a multimode cavity structure,[122] all

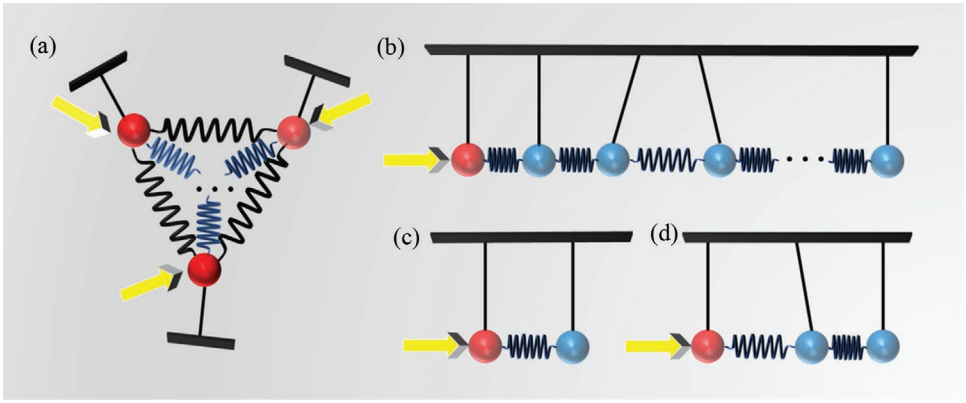

Figure 2. Coupled oscillator model for Fano resonance in photonic molecules. a) Schematic illustration of multiple coupled oscillators with each oscillator driven by an external force, in which all the oscillators interact with each other. b) Schematic illustration of multiple coupled oscillators with a driving force, in which each oscillator only interacts with the adjacent oscillators. c) Schematic illustration of two coupled oscillators with a driving force. d) Schematic illustration of three coupled oscillators with a driving force.

optical modes interact with the waveguide mode directly, and each optical mode in multimode cavity can be considered to be a oscillator with a driving force. The analytical theory based on the coupled oscillator model allows us to understand the Fano and EIT-like responses as a function of system parameters.

In another general case, multiple coupled oscillators are composed of a single bright resonator and multiple dark resonators, as shown in Figure 2b. The first resonator is driven by the external force $f(t)$, and all other resonators only interact with adjacent resonators.[119,121] The jth resonator is described by the excitation $p_j(t)$ (j = 1,2...N), and γ_j and ω_j are the damping factor and resonance frequency of the resonators. In the frequency domain, the multi-oscillator model can be described as

$$\begin{bmatrix} D_1 & \kappa_1 & 0 & \cdots & 0 \\ \kappa_1 & D_2 & \kappa_2 & & \vdots \\ 0 & \kappa_2 & \ddots & \ddots & 0 \\ \vdots & & \ddots & D_{N-1} & \kappa_{N-1} \\ 0 & \cdots & 0 & \kappa_{N-1} & D_N \end{bmatrix} \cdot \begin{bmatrix} p_1(\omega) \\ p_2(\omega) \\ \vdots \\ p_{N-1}(\omega) \\ p_N(\omega) \end{bmatrix} = \begin{bmatrix} f(\omega) \\ 0 \\ 0 \\ \vdots \\ 0 \end{bmatrix} \tag{4}$$

where $D_j = 1 - (\omega/\omega_j)^2 - i\gamma_j(\omega/\omega_j)$ (j = 1, 2,..., N), κ_m denotes the coupling strength between the mth cavity and the m + 1th cavity (m = 1, 2,..., N–1). From Equation (4), one can get

$$p_1(\omega) = \cfrac{f(\omega)}{D_1 - \cfrac{\kappa_1^2}{D_2 - \cfrac{\kappa_2^2}{\ddots \cfrac{}{D_{N-1} - \cfrac{\kappa_{N-1}^2}{D_N}}}}} \tag{5}$$

The surface conductivity σ_N, for the general system composed of a single bright resonator and multiple dark resonators, can be given as

$$\sigma_N = \cfrac{-i\omega}{D_1 - \cfrac{\kappa_1^2}{D_2 - \cfrac{\kappa_2^2}{\ddots \cfrac{}{D_{N-1} - \cfrac{\kappa_{N-1}^2}{D_N}}}}} \tag{6}$$

Substituting the wave impedance ζ and surface conductivity σ_N into Equation (3), the transmission coefficient, reflection coefficient and group delay can be effectively derived.[123] To simplify device design and control device size, the double-cavity and three-cavity photonic molecules have been widely proposed to realize Fano resonance,[120,121] which can be theoretically studied utilizing the two and three coupled oscillators model, as depicted in Figure 2c,d.

The theoretical derivations above are useful for describing the Fano phenomena in photonic molecules, covering single-cavity, double-cavity, three-cavity, and multiple-cavity structures, which performs as a guideline for controlling the spectral properties and designing photonic devices based on Fano resonance. The coupled oscillators model not only reveals the interactions between optical modes in photonic molecules, but also improves the understanding of Fano physics for other designs. To better account for and control the spectral characteristics of photonic molecules with multiple resonances and multiple ports, we will discuss several theoretical analyses based on the coupled mode theory in the following subsection.

3.2. Coupled Mode Theory

The coupled mode theory proposed for electromagnetism originates from the 1950's. The coupled resonators correspond to the coupling of modes in time, while the coupled waveguides correspond to the coupling of modes in space.[104] In 2003, based on the coupled mode theory, Fan et al. proposed a theoretical model for single-mode resonator with multiple input and output ports, as shown in **Figure 3**a. Both the direct and indirect pathways are incorporated in the theory, which is applicable to many configurations exhibiting the Fano effect.[103,105] In accordance with the energy-conservation and time-reversal symmetry, the theoretical model can be stated as

$$\frac{\mathrm{d}a}{\mathrm{d}t} = \left(-j\omega_0 - \frac{1}{\tau}\right)a + \langle K|s_+\rangle \tag{7}$$

$$|S_-\rangle = C|S_+\rangle + a|K\rangle \tag{8}$$

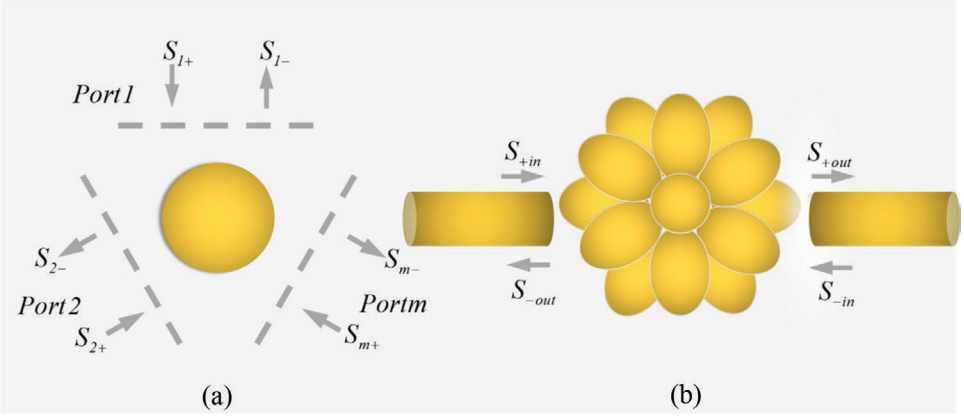

Figure 3. Coupled mode theory for Fano resonance in photonic molecules. a) Schematic of a resonator (cavity) coupled with multiple input and output ports. b) Sketch of multiple cavities side-coupled with two ports.

Equations (7) and (8) are the generalized form of coupled mode theory, in which a, ω_0, and τ denote the amplitude, resonance frequency, and lifetime of the resonance mode, respectively. The matrix C describes the direct coupling between incoming and outgoing waves in ports. $|S_-\rangle$ and $|S_+\rangle$ denote the outgoing and incoming waves. $|K\rangle$ represents the coupling coefficient between the resonator and the ports. $\langle K|$ is dependent on $|K\rangle$. The parameters $|S_-\rangle$, $|S_+\rangle$, $|K\rangle$, and $\langle K|$ can be expressed as

$$|S_+\rangle=\begin{pmatrix} s_{1+} \\ s_{2+} \\ \vdots \\ s_{N+} \end{pmatrix}, |S_-\rangle=\begin{pmatrix} s_{1-} \\ s_{2-} \\ \vdots \\ s_{N-} \end{pmatrix}, \quad |K\rangle=\begin{pmatrix} k_1 \\ k_2 \\ \vdots \\ k_N \end{pmatrix}, \quad \langle K|=\begin{pmatrix} k_1^* k_2^* \cdots k_N^* \end{pmatrix} \tag{9}$$

The relation between the incoming wave and the amplitude of resonant mode can be written as

$$a=\frac{\langle K|S_+\rangle}{j(\omega_0-\omega)+1/\tau} \tag{10}$$

Equations (7)–(10) are feasible for a single resonance mode coupling with multiple input and output ports.

According to Equations (7)–(10), the transmittance and reflectance of two-port structures can be derived as

$$T=\frac{\left[(\omega_0-\omega)t\pm\frac{r}{\tau}\right]^2}{(\omega_0-\omega)^2+\tau^{-2}}, \quad R=\frac{\left[(\omega_0-\omega)r\mp\frac{t}{\tau}\right]^2}{(\omega_0-\omega)^2+\tau^{-2}} \tag{11}$$

where the real constants r and t follow the relation $r^2 + t^2 = 1$, and the ± sign depends on the properties of the resonant mode. If $r = 0$ or $r = 1$, the system will exhibit Lorentzian line shape, otherwise, it will present an asymmetric Fano line shape.

When a multimode resonator couples with multiple ports, based on the coupled mode theory, the general theoretical model can be described as[90,103–107]

$$\frac{\mathrm{d}}{\mathrm{d}t}|a\rangle=-j\Omega|a\rangle-\Gamma_i|a\rangle+\Gamma_e|a\rangle+K^{\mathrm{T}}|S_+\rangle \tag{12}$$

$$|S_-\rangle=C|S_+\rangle+K|a\rangle \tag{13}$$

In this case, the resonator eigenmodes are orthogonal to each other. $|S_-\rangle$, $|S_+\rangle$, and $|a\rangle$ stand for the outgoing wave, incoming wave, and amplitude of the resonant mode, respectively.

In Equations (12) and (13), matrixes Ω, K, Γ_i and Γ_e, respectively, correspond to the resonance frequency, coupling coefficient between the resonant modes and ports, intrinsic loss rate, and external loss rate of the resonant modes. They can be expressed as

$$|a\rangle=\begin{pmatrix} a_1 \\ a_2 \\ \vdots \\ a_N \end{pmatrix}, |S_+\rangle=\begin{pmatrix} s_{1+} \\ s_{2+} \\ \vdots \\ s_{M+} \end{pmatrix}, |S_-\rangle=\begin{pmatrix} s_{1-} \\ s_{2-} \\ \vdots \\ s_{M-} \end{pmatrix} \tag{14}$$

$$K=\begin{bmatrix} \kappa_{11} & \kappa_{12} & \cdots & \kappa_{1N} \\ \kappa_{21} & \kappa_{22} & \cdots & \kappa_{2N} \\ \vdots & \vdots & \ddots & \vdots \\ \kappa_{M1} & \kappa_{M2} & \cdots & \kappa_{MN} \end{bmatrix}, \Omega=\begin{bmatrix} \omega_{11} & \omega_{12} & \cdots & \omega_{1N} \\ \omega_{21} & \omega_{22} & \cdots & \omega_{2N} \\ \vdots & \vdots & \ddots & \vdots \\ \omega_{N1} & \omega_{N2} & \cdots & \omega_{NN} \end{bmatrix} \tag{15}$$

$$\Gamma=\begin{bmatrix} \gamma_{i11} & \gamma_{i12} & \cdots & \gamma_{i1N} \\ \gamma_{i21} & \gamma_{i21} & \cdots & \gamma_{i2N} \\ \vdots & \vdots & \ddots & \vdots \\ \gamma_{iN1} & \gamma_{iN2} & \cdots & \gamma_{iNN} \end{bmatrix}, \Gamma_e=\begin{bmatrix} \gamma_{e11} & \gamma_{e12} & \cdots & \gamma_{e1N} \\ \gamma_{e21} & \gamma_{e22} & \cdots & \gamma_{e2N} \\ \vdots & \vdots & \ddots & \vdots \\ \gamma_{eN1} & \gamma_{eN2} & \cdots & \gamma_{eNN} \end{bmatrix}$$

Basing on the boundary conditions and Equations (12)–(15), one can get a theoretical model for the system, which consists of multiple single-mode cavities side-coupled with two symmetric ports,[90] as depicted in Figure 3b. The characteristic equations of which can be written as

$$\frac{\partial}{\partial t}|a\rangle=-j\Omega|a\rangle-\Gamma_i|a\rangle+\Gamma_e|a\rangle+S_{+\mathrm{in}}|K\rangle+S_{-\mathrm{in}}|K\rangle-M|a\rangle \tag{16}$$

$$S_{+\mathrm{out}}=S_{+\mathrm{in}}-\langle K|a\rangle \tag{17}$$

$$S_{-\mathrm{out}}=S_{-\mathrm{in}}-\langle K|a\rangle \tag{18}$$

$S_{\pm\mathrm{in}}$ and $S_{\pm\mathrm{out}}$ are the incoming and outgoing waves in the two ports, and Matrix M denotes the coupling coefficient between the optical modes in the interacting cavities, which are written as

$$|a\rangle=\begin{pmatrix} a_1 \\ a_2 \\ \vdots \\ a_N \end{pmatrix}, |K\rangle=\begin{pmatrix} k_1 \\ k_2 \\ \vdots \\ k_N \end{pmatrix}, \langle K|=\begin{pmatrix} k_1^* k_2^* \cdots k_N^* \end{pmatrix}, M=\begin{bmatrix} \mu_{11} & \mu_{12} & \cdots & \mu_{1N} \\ \mu_{21} & \mu_{22} & \cdots & \mu_{2N} \\ \vdots & \vdots & \ddots & \vdots \\ \mu_{N1} & \mu_{N2} & \cdots & \mu_{NN} \end{bmatrix} \tag{19}$$

where a_N is the amplitude of the resonant mode with resonance frequency ω_N, and k_N denotes the coupling between ports and cavities. In Equation (16), matrixes Ω, Γ_i, and Γ_e have the identical form with those in Equation (15). If $m \neq n$, $\omega_{mn} = 0$, $\gamma_{imn} = 0$, $\gamma_{emn} = 0$, and $\mu_{mn} = \omega_{nn}/(2Q_{mn})$; if $m = n$, $\omega_{mn} = \omega_m$, $\gamma_{imn} = \omega_{mn}/(2Q_{im})$, $\gamma_{emn} = \omega_{mn}/(2Q_{em})$, and $\mu_{mn} = 0$. Q_{im}, Q_{em}, and Q_{mn} denote cavity quality factors, which are in connection with intrinsic loss, port coupling loss, and direct coupling between the mth and nth modes. Using Equations (15)–(19) and boundary conditions, one can derive the transmittance of a structured photonic molecule system. When aligning the optical cavities in various configurations, the spectral properties are closely related to the number of optical cavities, symmetry and topology of photonic molecules. The validity of the theoretical model is confirmed by comparing with the simulation and experimental results. The coupled mode theory promises insight into modes interactions in time, and can accurately describe the fascinating electromagnetic oscillation in photonic molecules.[37,38,83,86,103–107,124–126]

4. Classification of Photonic Molecules Generating Fano Resonance

In recent years, photonic molecules consisting of optical microcavities have emerged as a key building block for high performance photonic devices from the perspective of both fundamental science and practical applications.[38,127–131] Typical optical microcavities used for Fano resonance realization include whispering-gallery-mode, plasmonic, Fabry–Pérot (FP),

and photonic crystal cavities.[37,38,83,114] Assembling optical cavities in a wide range of structures, various artificial photonic molecules configurations have enabled the Fano resonance and brought forth the development of highly integrated photonic circuit.

4.1. Single-Cavity Photonic Molecule

In a single multimode cavity, the optical modes are orthogonal with each other generally. The waveguide induces indirect coupling between optical modes, which introduces Fano resonance resulting from the interference between the different pathways. Xiao et al. studied the transmission spectra of a fiber coupled with a single pilydimethylsiloxane (PDMS)-coated silica microtoroid, which supports two whispering-gallery modes (WGMs) with distinct thermal response versus temperatures. The detuning between the probe mode and control mode can be tuned by temperature. Due to the different thermo-optic coefficients between PDMS-coated silica, the probe mode presents a blueshift, while the control mode experiences a redshift. With increased temperature, the transmission spectra exhibit mutual transformation of EIT and Fano resonance.[111]

The spectra lineshape in a silica microtoroid can also be adjusted by the fiber-cavity coupling distance and the polarization of incident light. As the polarization of incident light is changed, the asymmetric Fano resonance lineshape converts into a symmetric Lorentzian line shape, as shown in **Figure 4**a. It was proposed that the quasi-TE or quasi-TM modes in the microtoroid are neither exactly vertically nor parallelly polarized.[112] When the incident polarization is vertical to the low-Q mode, the microtoroid only supports high-Q mode, which results in a Lorentzian lineshape. In a slightly deformed silica microtoroid excited by a free-space laser beam,[132] the induced transparency in the measured transmission spectra arises from the coupling of continuous chaos and discrete regular modes. As the optical beam is moved from the top to the bottom, the induced transparency transforms into asymmetric Fano line shape, as shown in Figure 4b.

Rapid developments in photonic technology has enabled the metal-insulator-metal (MIM) waveguide as a platform for realizing on-chip photonic integrated circuits.[133] Figure 4c displays double Fano resonances in a single defect cavity side-coupled with a MIM waveguide. One is attributed to the higher-order mode excited in rectangular cavity with a small stub, while the other is related to the lower-order mode in stub. Thus, the two Fano resonances exhibit different responses versus structural parameters. Increasing the stub depth, the high-energy Fano resonance remains nearly unchanged, while the low-energy Fano resonance shifts toward longer wavelength. The double Fano resonances originating from different mechanisms have potential applications in self-reference accurate sensing in complex environments.[134] Li and co-workers also have numerically and analytically investigated the Fano resonance in MIM waveguide with a multimode stub cavity, and demonstrated optical transmission evolution versus aspect ratio.[63,135] A single symmetry breaking ring cavity could also facilitate the realization of Fano resonance and provides a new degree of freedom to modulate the spectra characteristics.[136] However, to date, realizing the ultracompact on-chip plasmonic circuits is still a great challenge. Chai et al. experimentally demonstrated on-chip Fano resonance in a single plasmonic composite nanocavity covered with an 80 nm thick poly (methyl methacrylate) (PMMA) layer.[137] The composite cavity composed of two crossed nanogrooves is side-coupled to a bus waveguide, as shown in Figure 4d. The transmission spectra in the near-infrared range present blue-shift with the ambient temperature increase from 25 to 80 °C.

Differing from the multimode cavity, the single-mode cavity configurations typically exhibit transmission or refection spectra with symmetric Lorentzian or quasi-Lorentzian line shape. Therefore, partially reflecting elements have been adopted to produce Fano resonance. Fan analytically demonstrated asymmetric Fano resonance by using two partially reflecting elements in waveguide side-coupled to a cavity.[109] The two partially reflecting elements function as a Fabry–Pérot cavity. To give evidence of the analytical theory, they investigated the spectral properties in the photonic crystal structure shown in Figure 4e. A row of dielectric rods are removed to form a waveguide, and the radius of a single rod is reduced to introduce a cavity. Two small cylinders in the waveguide act as partially reflecting elements. The transmission responses exhibit asymmetric Fano lineshape. In addition, the interaction between the discrete state in the photonic crystal cavity and continuum state in the line-defect waveguide with one blockade hole can also give rise to Fano resonance, as shown in Figure 4f. The inserted hole breaks the mirror symmetry and serves as a partially transmitting element.[138,139] Compared with the cascaded cavity systems, the device alleviates the requirement of matching several resonances and reduces the required precision of the fabrication process.[138] The experimental transmission spectra in photonic crystal structures are consistent with the analytical results and the on–off contrast achieved 40 dB.

In addition to the above mentioned optical microcavity, some other single-cavity-based structures have also been proposed to demonstrate the Fano resonance line shape. Shang et al. experimentally investigated the spectral responses, in an aqueous environment, of a sausage-like microresonator coupled with a fiber taper, as shown in Figure 4g. Adjusting the coupling position between the fiber taper and sausage-like microresonator, the spectra line shape evolves periodically, and the asymmetric Fano resonance line shapes appear in the transmission spectra.[140] More interestingly, Lorentzian, EIT and Fano line shapes can be achieved in a microring coupled to a waveguide inserted with two air-holes, as illustrated in Figure 4h.[141] At the resonant frequencies of microring cavity, modulating the distance between two air-holes causes the transformations among different resonance line shapes. Averaged over tens of devices, the extinction ratios and slope rates in Fano line shapes achieved 20 dB and 280 dB nm^{-1}, respectively.

4.2. Double-Cavity Photonic Molecule

For double-cavity photonic molecule producing Fano resonance, the cavities directly couple with each other via the evanescent field, or different cavities couple indirectly through common waveguide. In 2006, Xu et al. first experimentally demonstrated

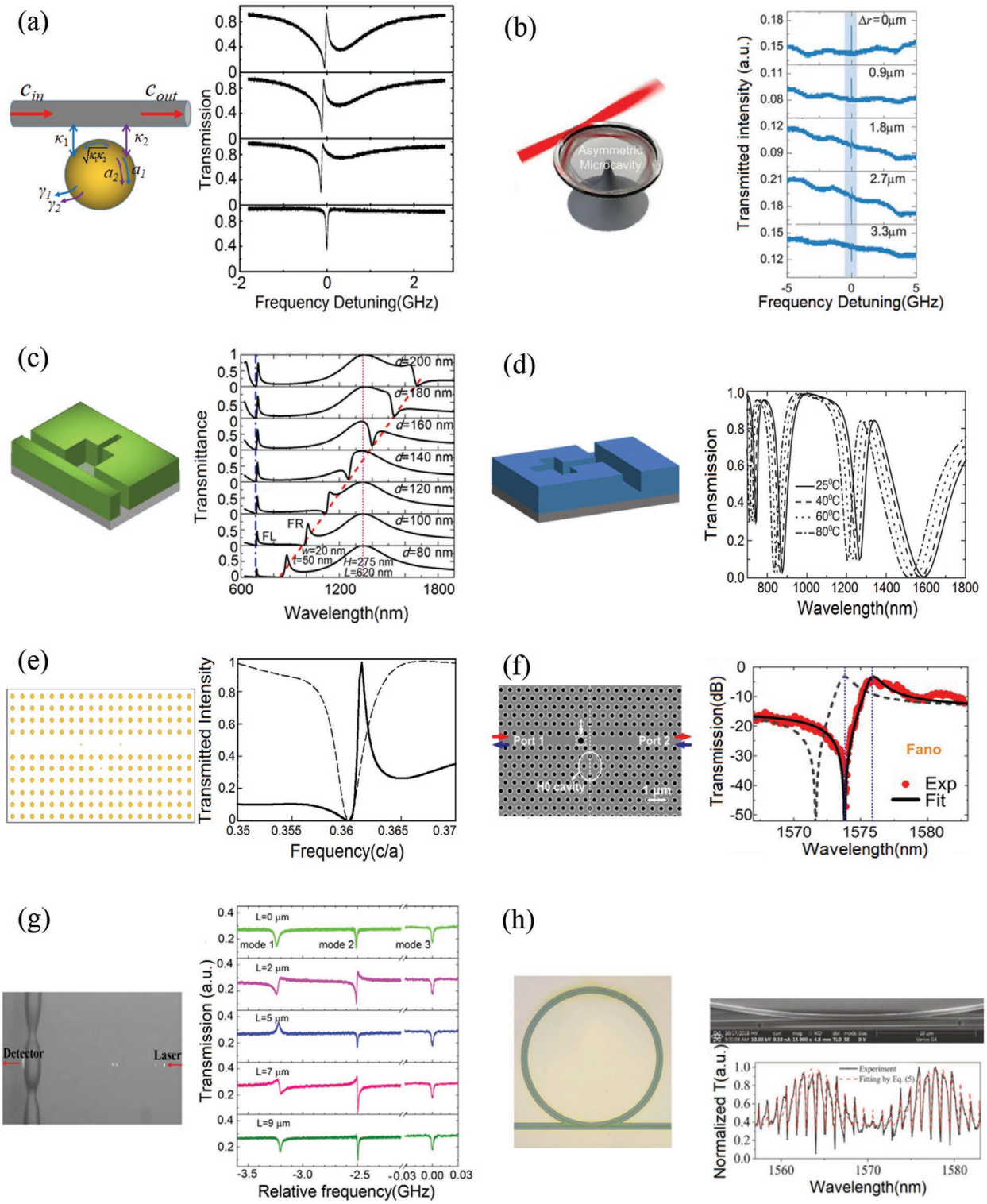

Figure 4. Fano resonance in single-cavity photonic molecule structures. a) Schematic of a fiber taper coupled with a toroidal microcavity and transmission spectra versus polarization of the incident light. b) A deformed silica microtoroid excited by a focused beam and measured transmission spectra versus the position of focused free-space laser beam. c) A defect nanocavity side-coupled with a plasmonic waveguide and transmission spectra versus small stub depth. d) A single composite nanocavity side-coupled to a plasmonic waveguide and the calculated transmission spectra of the plasmonic structure covered with PMMA layer versus ambient temperature. e) A photonic crystal cavity coupled to a photonic crystal waveguide, in which the solid line denotes the transmission spectra of the photonic crystal structure. Two small cylinders enable partial reflection of waveguide modes. The dashed line exhibits the transmission spectra for the corresponding photonic crystal structure without two partially reflecting rods in the waveguide. f) SEM image of photonic crystal structure, which consists of a point defect cavity (H0-type) coupled to a line defect waveguide. Measured (red dots) and theoretical fitting (black solid line) transmission spectra.

the phenomena of on-chip EIT-like spectra in coupled silicon ring resonators, which were fabricated on a silicon-on-insulator substrate.[142] The diameters of the silicon ring cavities were 10 μm. Slight difference in diameter was introduced to detune the two ring cavities. The transmission spectra exhibit asymmetric line shapes with varying cavity separations, as shown in **Figure 5**a. However, the footprint of the silicon ring cavity photonic molecule reaches hundreds of square microns. Thus, it is desirable to construct photonic molecules of a smaller size, and various plasmonic double-cavity photonic molecule structures have been investigated to achieve Fano resonance in recent years.

Han et al. realized EIT using two detuned cavities aperture-side-coupled to a MIM waveguide.[143] They numerically showed that the footprint of the designed plamonic system can be smaller than 0.15 μm^2. Based on EIT, the dispersion relation in the plasmonic waveguide system was also investigated, which is composed of a periodic array of two stub resonators side-coupled to a metal-dielectric-metal (MDM) waveguide.[92] The slow-down factor and slow light bandwidth are dependent on the detuned frequency between cavities. Figure 5b presents Fano resonance in the strong-confinement MIM waveguide side-coupled with two rectangular cavities.[144] The Fano line shape is attributed to the coherent interference between resonance modes with different resonance frequencies and coupling rates. The cavity with weak coupling rate supports discrete state, while the other cavity with a strong coupling rate supports a quasi-continuum state. Moreover, the cavity-cavity separation has significant influences on the reflection spectrum. In a plasmonic MIM waveguide side-coupled to double stub resonators with direct coupling, there is a trade-off between coupling quality factor and coupling coefficient. The coupling strength and phase difference contribute to the change of transparent bandwidth and degree of symmetry of the spectral line shape, respectively.[15]

When a MIM waveguide couples to a single-mode cavity and a multimode cavity, the transmission spectra possess dual EIT effects, and the evolution tendencies of two transparent peaks differ from each other as the depth of stub resonators is increased.[145] Three Fano resonances arise in a plasmonic system composed of two circular cavities.[146] One is attributed to the interference between optical modes in one resonator, the other is owning to the interference between optical modes in two resonators, and the third Fano resonance originates from the interference between degenerate modes, each of which is described by distinct transmission coefficients.[146] Due to different mechanisms, the three Fano resonances can be modulated independently or semi-independently, as depicted in Figure 5c.

For the plasmonic double-cavity photonic molecule structure mentioned above, the ohmic losses of metal prevent the practical applications to photonic devices. The plasmonic cavities have low quality factors, and the channel spectral density is orders of magnitude lower than that of dielectric cavities. Thus, many kinds of dielectric cavities have been utilized to realize Fano resonance, including photonic crystal microcavities, silica microtoroid,[147] silicon ring cavities.[148] However, the feature sizes of dielectric cavities are usually several microns, which limits the realization of highly integrated on-chip photonic circuits. To ensure small propagation losses and a large group index, a hybrid nanostructure in Figure 5d was proposed, which is composed of plasmon–photon hybrid nanocavity and waveguide.[149] Compared with the plasmonic slot waveguide, the propagation loss of the plasmon–photon hybrid waveguide is considerably lower. The destructive interference of the plasmonic cavity and photonic crystal cavity modes, in the plasmon–photon hybrid nanostructure, enables the formation of an EIT-like effect.

To study the Fano phenomena in the above photonic molecule schemes, the bus waveguide is an indispensable component. The large loss-detuning between the two cavities or only the lower quality factor cavity coupled to waveguide may influence the results and reduce the accuracy of any conclusions. To overcome these disadvantages, Caselli et al. substituted a near-field probe for the waveguide,[150] and introduced a family of generalized Fano profiles to demonstrate the optical responses of coupled modes in the proximity of the exceptional point singularity. Through the detection of generalized Fano lineshapes, the ability of the near-field configuration to characterize the transition across the exceptional point was demonstrated. The experimental Fano profiles agree well with the finite-difference time-domain simulations. The generalized Fano profiles play an important role in spectroscopy and material science, not only involving the optical responses but also electronic properties.

4.3. Multiple-Cavity Photonic Molecule

In multiple-cavity photonic molecule, three or more assembled cavities interact with each other, introducing more degrees of freedom to control the spectral signatures.[98–101] In 2009, via multiple coupled photonic crystal cavities, Yang et al. were the first to experimentally observe the resonance and phase controlled EIT-like phenomena, as shown in **Figure 6**a. Two pump beams were used to perturb the resonance wavelengths of cavities 2 and 3. As the pump power of the laser focused on cavity3 is increased, the resonance wavelength of cavity3 presents a red shift, and the resonance detuning between cavity2 and cavity3 decreases. Hence, cavity2 and cavity3 interact with each other more strongly, and the short wavelength transparency window narrows progressively. Figure 6a also shows the phase shift for

The blockade hole in the waveguide acts as partially transmitting element denoted by the dashed square. g) The micrograph of a sausage-like microresonator in water and experimental transmission spectra (from top to bottom) with the sausage-like microresonator moved to the left along fiber taper. h) Optical micrograph of a microring resonator coupled with waveguide. The SEM image of the waveguide-microring coupling region with two air-holes inserted in bus waveguide. Measured transmission spectrum (black line) and fitting result (red dashed line) of the fabricated device. a) Reproduced with permission.[112] Copyright 2011, American Institute of Physics. b) Reproduced with permission.[132] Copyright 2013, Wiley-VCH. c) Reproduced with permission.[134] Copyright 2014, The Optical Society. d) Reproduced with permission.[137] Copyright 2014, Wiley-VCH. e) Reproduced with permission.[109] Copyright 2002, American Institute of Physics (AIP). f) Reproduced with permission.[138] Copyright 2015, Wiley-VCH. g) Reproduced with permission.[140] Copyright 2017, The Optical Society. h) Reproduced with permission.[141] Copyright 2019, Walter de Gruyter.

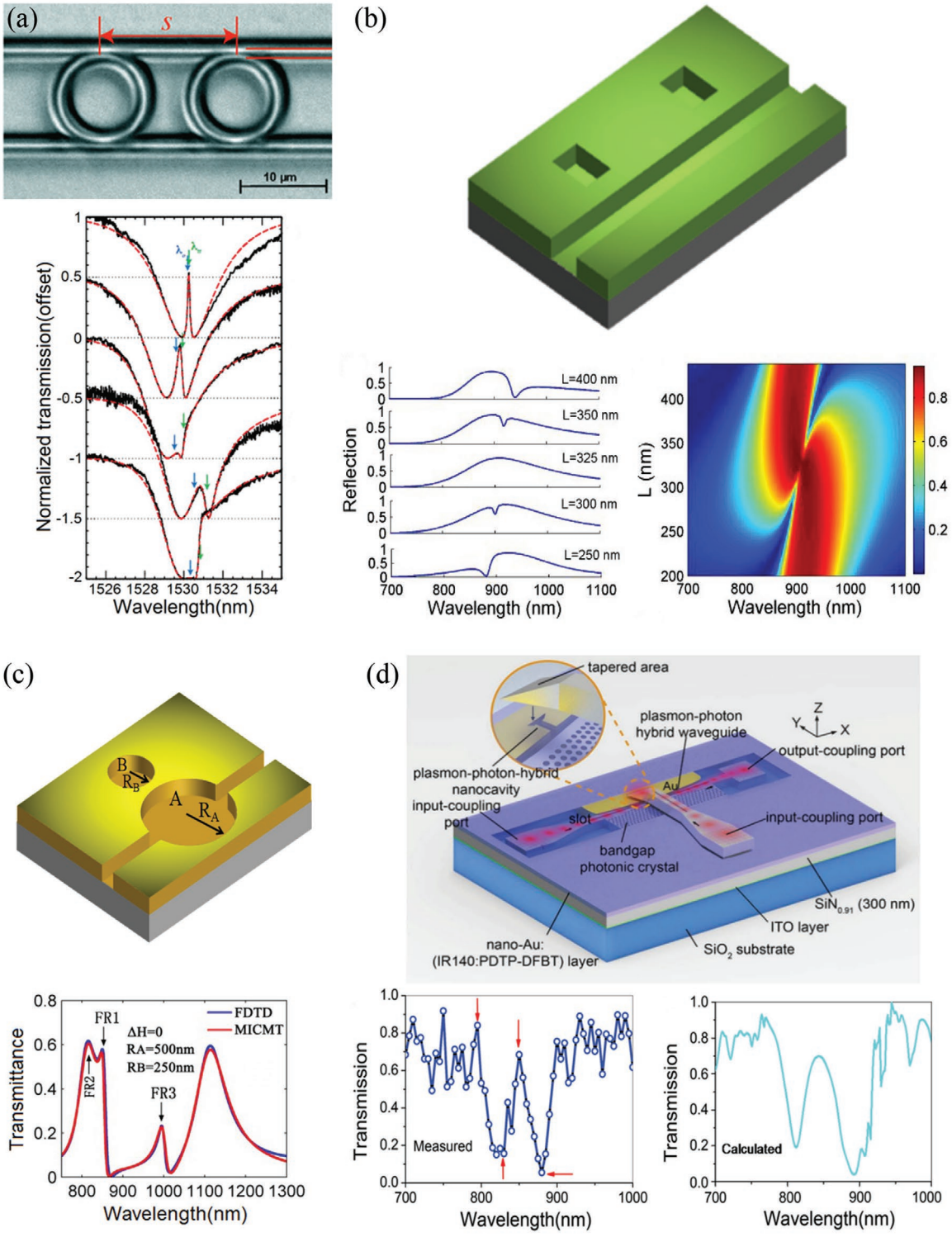

Figure 5. Fano resonance in double-cavity photonic molecule structures. a) Optical micrograph of the silicon ring resonator coupled to parallel waveguides. Experimental transmission spectra (black solid line) and theoretical fits (red dashed line) versus ring separation *s* for the microring resonator system. b) Schematic of the MDM dual-resonator-coupled waveguide and reflection spectra versus cavity–cavity separation. c) A system composed of two circular cavities and two MDM waveguides. The FDTD (blue line) and multimode interference coupled mode theory (MICMT) results (red line) of the transmission spectra of the plasmonic system. d) Schematic of plasmon–photon hybrid nanostructure and corresponding measured and calculated transmission spectra. a) Reproduced with permission.[142] Copyright 2006, American Physical Society. b) Reproduced with permission.[144] Copyright 2012, The Optical Society. c) Reproduced with permission.[146] Copyright 2017, The Optical Society. d) Reproduced with permission.[149] Copyright 2016, Wiley-VCH.

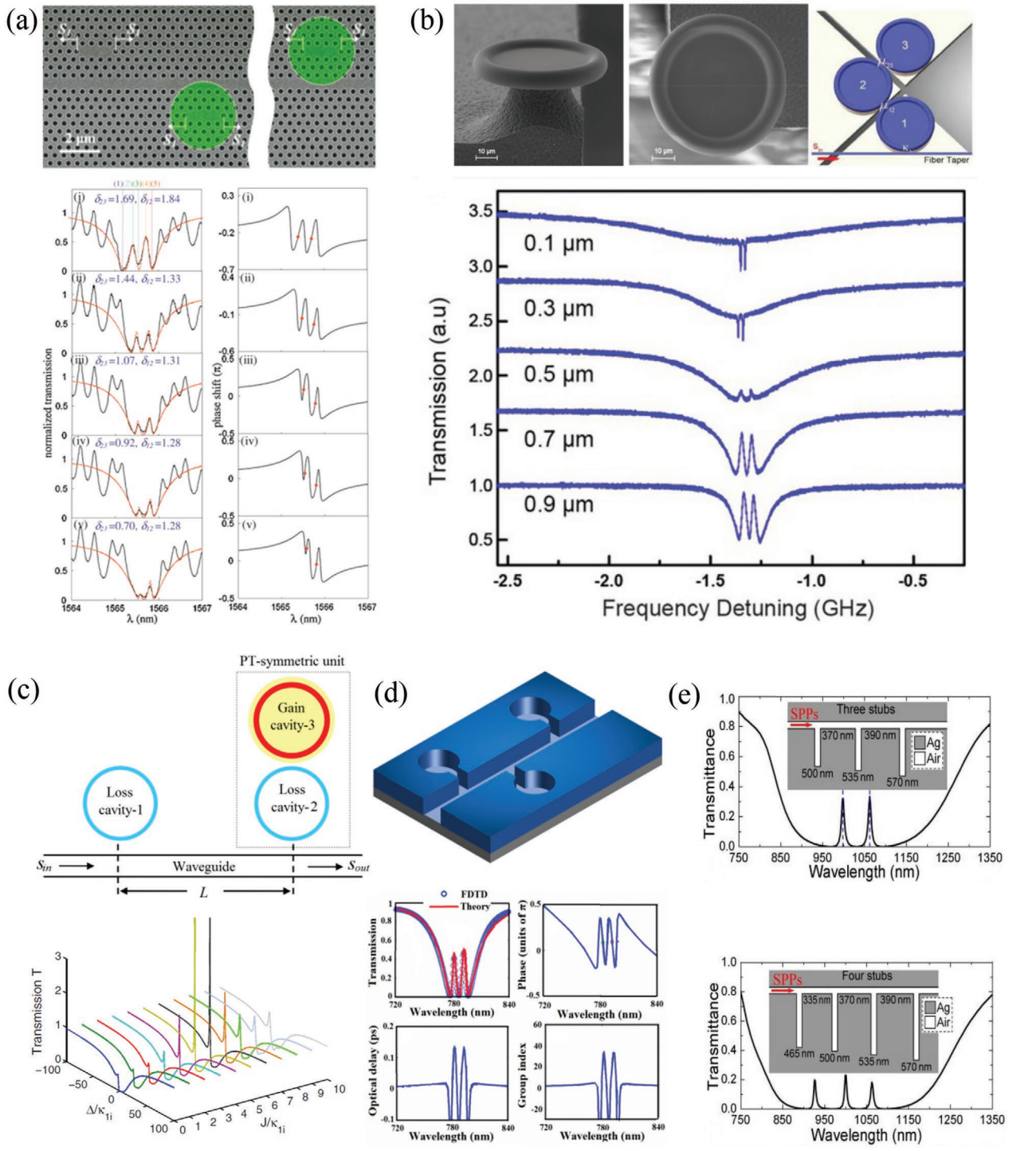

Figure 6. Fano resonance in multiple-cavity photonic molecule structures. a) SEM image of multiple photonic crystal cavities. Measured and theoretical transmission spectra and corresponding transmission phase shift versus detuning δ_{12} and δ_{23}. b) Top: SEM images of side view and top view of the microtoroid, and the configurations of the triple-cavity photonic molecule. Bottom: the transmission spectra as a function of distance between the fiber and cavity1. c) Sketch of PT-assisted triple-cavity configuration and transmission spectra versus the detuning $\Delta/\kappa_1 i$ for different intercavity coupling strengths $J/\kappa_1 i$. d) Schematic of multiple nanodisk cavities aperture-side-coupled to a MIM waveguide. Numerical (circles) and theoretical (solid curve) transmission spectra in the triple-cavity coupled waveguide structure, and corresponding transmission phase shift, optical delay line, and group index around the transparent windows. e) Top: transmission spectrum and schematic of the triple-cavity photonic molecule system. Bottom: transmission spectrum and schematic of the four-cavity photonic molecule configuration. a) Reproduced with permission.[151] Copyright 2009, American Physical Society. b) Reproduced with permission.[152] Copyright 2017, Wiley-VCH. c) Reproduced with permission.[159] Copyright 2017, American Physical Society. d) Reproduced with permission.[161] Copyright 2012, American Physical Society. e) Reproduced with permission.[162] Copyright 2012, The Optical Society.

the double EIT-like responses, and indicates that the stronger coupling will induce larger optical delays.[151]

Three independently-selectable ultrahigh quality microtoroids provide a platform to explore topologically protected photonic states and analogies to quantum-optics.[152] Typical double EIT-like spectra of the coupled triple-cavity photonic molecule can be modulated by changing the cavity-cavity coupling strengths, resonance frequencies and coupling distance between the tapered optical fiber and cavities, as shown in Figure 6b. By tuning the polarizations of the three resonant modes, the transmission spectra will change into asymmetric line shape.[152,153] Decreasing the distance between the optical fiber and cavity1, the double EIT will evolve into double electromagnetically-induced absorption phenomena. Xiao and coworkers have also proposed a theoretical analysis of the spectral characteristics and energy distributions in triple-cavity photonic molecule structure.[154] They analyzed the evolution of supermode linewidths and frequencies, and established a superposition picture for the supermodes of triple-cavity photonic molecule structure. Moreover, in the flexible triple-cavity photonic molecule, the anomalous properties of the central supermode and EIT-like phenomena were demonstrated.

Since 1998, parity-time (PT) symmetry has become an active research topic.[155–158] Introducing PT symmetry into photonic structure can dramatically improve the performances of devices and stimulate further breakthroughs in photonics. Li et al. investigated the asymmetric Fano line shapes of the triple-cavity platform with local parity-time symmetry, as shown in Figure 6c.[159] In this structure, a single cavity is indirectly coupled to PT-symmetric coupled cavities via a bus waveguide. They presented the transmission properties of the PT-assisted triple-cavity versus the coupling strength between loss cavity2 and gain cavity3. It can be found that the asymmetric spectral line shapes are correlated to the cavity coupling strength in the PT-assisted configuration. Compared to the system of two indirectly coupled cavities, the PT-symmetric unit significantly enhances the extinction ratio and the slope of the Fano line shapes. The results pave the way toward utilizing the PT symmetry to study Fano resonance. In addition, more interestingly, Li et al. also demonstrated the multiple-Fano resonance via a coupled-cavity-array arrangement, which is similar to Ramsey absorption spectroscopy in atomic and molecular systems.[160] Therefore, they accordingly defined the multiple-Fano resonance phenomena as Ramsey-Fano resonance, which emerges from multiple quantum interference among various light pathways. Both the numbers of Fano peak and dip in the transmission spectra are closely related to the cavity number *N*.

Surface plasmon polaritons (SPPs), which can break the classical diffraction limit and confine the electromagnetic radiation in nanoscale domain, may facilitate hybrid integration between photonics and electronics. Thus, to further reduce device size, multiple EIT-like phenomena were investigated in a multiple-cavity photonic molecule structure composed of multiple nanodisk cavities aperture-side-coupled to a plasmonic waveguide, as depicted in Figure 6d.[161] The plasmonic waveguide coupled with *N* resonators can realize *N*–1 transparent windows and multi-area with slow-light effect. Chen et al. studied the multiple plasmon-induced transparencies in a plasmonic waveguide coupled with series of stub cavities. The constructed three-coupled-resonator and four-coupled-resonator systems, respectively, are shown in Figure 6e.[162] The footprint of the plasmonic structure is only ≈0.6 μm^2. Moreover, the phase-coupled effect plays a vital role in the EIT-like phenomena, and the FWHM of the transparent peaks is much narrower than that of a single stub resonator. The spectral responses of the ultracompact structure hold potential applications in complex functional optical devices, such as switching, sensing and light storing.

5. Applications of Fano Resonance

The intriguing features of Fano resonance in photonic molecules enable numerous novel applications. In this section, we will introduce recent progress in several interesting applications such as sensing, switching and nonreciprocal propagation.

5.1. Sensing

Optical sensing, with characteristics of high sensitivity, high of merit, small footprint, and low detection limit, is desirable for highly integrated photonic circuits. The narrow linewidth and large spectral contrast of Fano resonance promise the realization of high-performance optical sensors. Moreover, the normal dispersion around the Fano resonance gives rise to a decrease in the group velocity, which enhances the field intensity and light–matter interaction, significantly improving the sensitivity to the variations in the surrounding environment. In particular, the sensing based on the asymmetrical Fano resonance with photonic molecules has attracted extensive research interest in recent years.

Xiao et al. theoretically investigated the sensing applications of Fano resonance supported by coupled microcavities, as shown in **Figure 7**a. At fixed wavelength, the asymmetrical transmission spectrum changes much faster than the Lorentzian profile in a single cavity resonance and, thereby, increases the sensitivity to refractive index changes.[39] Considering the coupled cavities as a composite cavity, a theoretical model was established to study the spectral features of the plasmonic stub-pair structure.[90] The detection sensitivity approaches 6.541×10^7 m^{-1} and offers an order of magnitude enhancement over the single stub case. Based on the phase modulation, a plasmonic sensor design was proposed for fixed band detection,[163] as shown in Figure 7b. Even when increasing the refractive index of analyte, the working bandwidth remains unchanged and is twice as narrow as that of the commonly used approach for the same analyte.[163] Besides, local parity-time symmetry can be used to tune the Fano line shape to increase the slope to improve the sensitivity of the refractive index sensor.[159] Compared to the two indirectly coupled lossy cavities, the best sensitivity is five orders magnitude larger.

5.2. Optical Switching

Optical switching, similar to electronic switching, performs the function of controlling optical signals, which plays a crucial role in quantum information processing chip-scale devices, optical

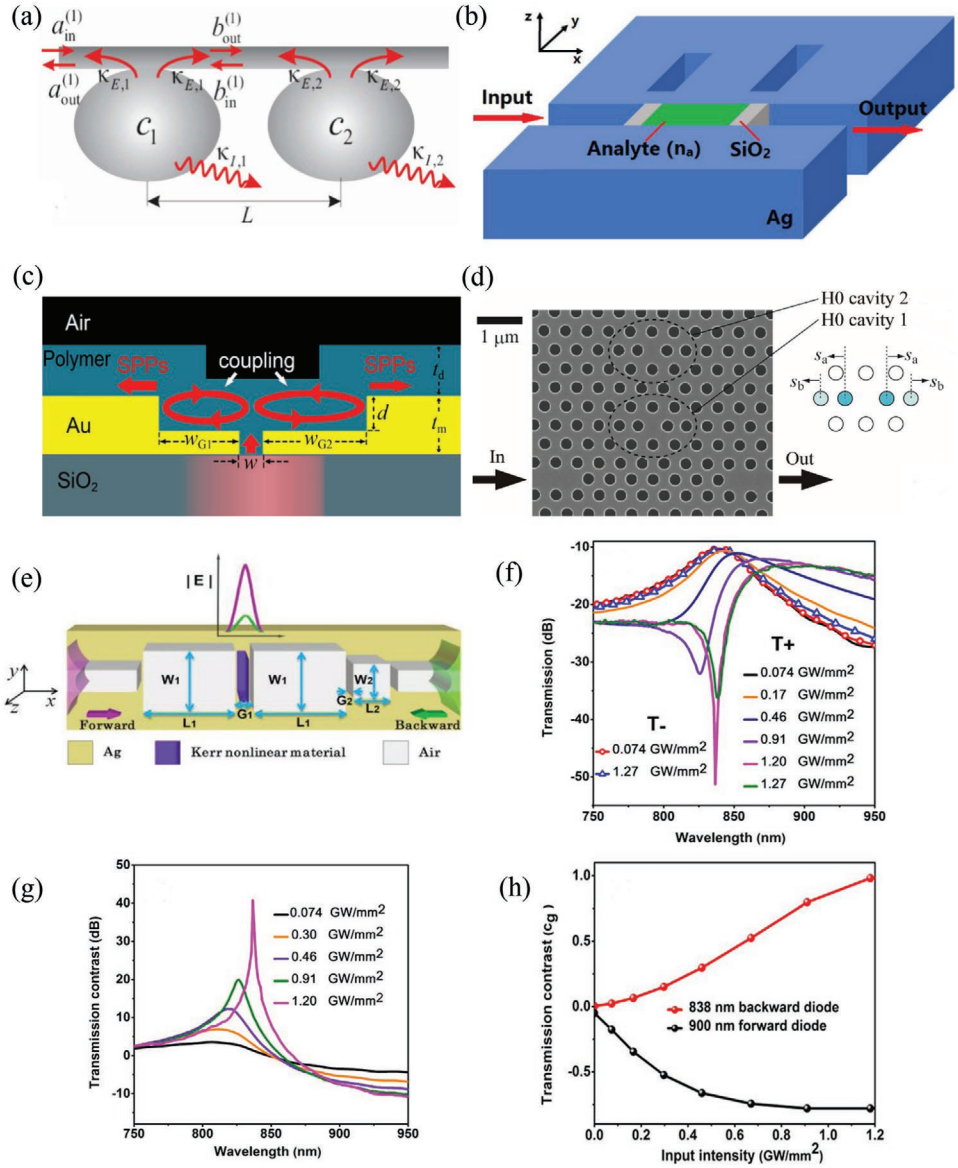

Figure 7. Applications of Fano resonance in photonic molecules. a) Schematic illustration of two coupled cavities for refractometric sensing. b) Sketch of plasmonic refractive index sensor with two silica walls inserted into the bus waveguide. c) Optical switching based on asymmetric T-shape single slit. d) SEM image of photonic crystal nanocavity based system used as an optical switch. e) Schematic of the optical plasmonic diode. f) Spectral responses and g) contrast ratio of forward (T_+) and backward (T_-) transmittance versus different input intensities. h) Contrast ratio for the forward diode (working at 900 nm) and backward diode (working at 838 nm). a) Reproduced with permission.[39] Copyright 2008, The Optical Society. b) Reproduced with permission.[163] Copyright 2019, Institute of Electrical and Electronics Engineers. c) Reproduced with permission.[165] Copyright 2013, Springer Nature. d) Reproduced with permission.[170] Copyright 2013, The Optical Society. e–h) Reproduced with permission.[174] Copyright 2015, The Optical Society.

communication networks and logic computing chips.[164] Therefore, considerable efforts have been devoted to realize optical switches[165–169] with low energy consumption, fast response times, broadband operation and high switching contrast. However, realizing an optical switching device with all the above key characteristics is still a great challenge. Compared with Lorentzian resonance, Fano resonance exhibiting sharp asymmetric profiles only requires a small shift in spectrum to obtain a high contrast, which lays the basis for optical switching devices.

Based on an asymmetric T-shape slit, a bidirectional switch was experimentally demonstrated, as shown in Figure 7c. The Fano features and field enhancement effects are exhibited in the plasmonic symmetry-breaking structure with lateral dimension smaller than 1 μm, and the on/off ratio is larger than 6 dB.[165] Chai et al. reported a low power, fast, and on-chip optical switch with a pump intensity of 450 kW cm^{-2}, 63 ps response time and multiple operating wavelengths, which is consisted of plasmon–photon hybrid nanostructures covered with nonlinear nanocomposite material.[149] For coupled photonic crystal cavities, Nozaki et al. experimentally and theoretically studied an optical switch based on Fano resonance, which presents better performances than a single cavity in terms of operation

bandwidth, contrast and switching energy,[170] as depicted in Figure 7d. The system composed of coupled InGaAsP-H0 cavities exhibits a sharp asymmetric line shape with a large contrast of nearly 20 dB. Owning to the steep slope and strong carrier-induced nonlinearity, an optical switch with pump energy of 1 fJ, response time of 18 ps and contrast of exceeding 10 dB was accessible. In addition, for a well-designed and fabricated coupled cavities structure, an optical switching device, with sub-femtojoule energy, a 20 dB contrast and 10 Gb s^{-1} bandwidth, was achievable.[170]

5.3. Nonreciprocal Propagation

Similar to the diodes, nonreciprocal propagation optical devices support a high contrast rate between the transmission intensities of two directional optical signals, and play a key role in all-optical signal processing units, optical interconnects and optical logic computing networks. The nonreciprocal transmission of light can be realized by breaking the time-reversal and spatial-reversal symmetries.[18] It was proposed that Fano resonance is one of the best ways to enhance the transmission contrast rate.[138,171–173]

Based on Fano resonance, Fan et al. proposed a tunable optical plasmonic diode in a nonlinear system, composed of three cavities inserted into MIM waveguides, as shown in Figure 7e.[174] The third cavity breaks the spatial symmetry of the system, which enables the nonreciprocal nonlinear response. In Figure 7f, as the input intensity increases from 0.74 to 1.20 GW mm^{-2}, the transmission peak for forward incidence presents red shift, while the transmission peak for backward incidence remains unchanged. The maximum transmission contrast ratio achieved in Figure 7g is 41.46 dB. Moreover, the plasmonic structure may also serve as forward or backward diode for different input wavelengths, as depicted in Figure 7h.[174] An on-chip optical diode was experimentally realized using plasmonic waveguide coupled to two composite nanocavities. The threshold intensity is 145 μW, and the transmission contrast ratio approaches 15 dB.[18] In addition, a photonic molecule Fano structure with broken spatial symmetry also demonstrated nonreciprocal transmission characteristics at a bit rate of 10 Gbit s^{-1} and energy consumption of 4.5 fJ bit^{-1}.[138] The applications discussed here pave the way toward high-density photonic integrated circuits.

6. Conclusions and Outlook

With the advances in nano-optics and nanotechnology, photonic molecules are vital components for miniaturizing photonic devices and demonstrate impressive benefits for on-chip data communication and design configurability. The unique properties of the Fano line shape have been theoretically and experimentally studied in a variety of photonic molecules, including single-cavity, double-cavity, and multiple-cavity molecules. The physics and theoretical model for Fano features in photonic molecules represent a means to achieve on-chip control of light. Through programmable photonic molecules, different photonic devices employing Fano resonance, including biological sensors, switches, modulators, diodes, and buffers, are being actively investigated, and a considerable number of breakthroughs in theoretical, experimental, and technological studies have been reported. The fast, compact, and power-efficient nanolasers are a vital tool for reducing the size of photonic circuits.[175,176] The sharp Fano resonance with its properties of small linewidth and large field enhancement provides an advantageous building block for fabricating nanolasers. Moreover, the multiparameters self-reference,[86] multifunctional, compact Fano sensors render an effective approach to enable next-generation ultrahigh-sensitivity biosensors. However, to further improve the performance and robustness of photonic devices based on Fano-resonant photonic molecules, many highly challenging problems yet to be solved.

Ohmic losses, which decrease the sharpness of Fano profile, continue to hinder the applications of plasmonic–photonic molecules.[83,86–88] Parity-time symmetry may provide a new degree of freedom for creating novel plasmonic functional devices, and the loss in plasmonic structure can be compensated by the gain medium.[83,126,155,156] The gain, loss and interplay between the elements play essential roles in realizing PT symmetric photonic structure.

Double-cavity molecules and multiple-cavity molecules can increase the degrees of freedom for designing photonic devices.[97–99,177] Realizing tunable artificial photonic molecules may enable dynamic control of Fano features and enable future photonic devices.[97,125,178] However, how to dynamically and rapidly modulate the resonant frequencies of cavities, coupling strengths between optical cavities, and coupling between waveguide and cavity remains a significant challenge and is a promising area for future research.

The asymmetric and ultra-sharp Fano line shape is geometry- and environment-sensitive, offering a solution for highly accurate sensors. Unfortunately, guaranteeing the performance advantages requires exceptional fabrication technologies, and the inevitable flaws resulting from current technologies could compromise the Fano spectral signature of the device.[85,127,155] Topological effects could preserve the bright mode and dark mode even in the presence of structural flaws.[179,180] Thus, topologically protected Fano resonance is immune to structural flaws, and is currently the most promising means to achieve novel phonic devices with the superior robustness.

Acknowledgements

G.C. and S.D. contributed equally to this work. The authors are grateful to Dr. Guangwei Hu for fruitful discussion and assistance. This work was financially supported by the National Natural Science Foundation of China (Grant Nos. 61974144, 11564014, and 61865006), Guangdong Province Key Research and Development Plan (Grant No. 2019B010138002), the Natural Science Foundation of Hunan Province (Grant No. 2019JJ50481), the Education Department of Hunan Province (Grant No. 18B324), and the Xiangxi Autonomous Prefecture Science and Technology Program (Grant No. 2018SF5024). This article is part of the *Advanced Optical Materials* Hall of Fame article series, which recognizes the excellent contributions of leading researchers to the field of optical materials science.

Conflict of Interest

The authors declare no conflict of interest.

Keywords

coupled mode theory, coupled oscillator model, Fano resonance, optical cavities, photonic molecules

Received: December 25, 2019
Revised: February 10, 2020
Published online: March 23, 2020

[1] U. Fano, *Phys. Rev.* **1961**, *124*, 1866.
[2] A. E. Miroshnichenko, S. Flach, Y. S. Kivshar, *Rev. Mod. Phys.* **2010**, *82*, 2257.
[3] B. Luk'yanchuk, N. I. Zheludev, S. A. Maier, N. J. Halas, P. Nordlander, H. Giessen, C. T. Chong, *Nat. Mater.* **2010**, *9*, 707.
[4] N. Verellen, Y. Sonnefraud, H. Sobhani, F. Hao, V. V. Moshchalkov, P. V. Dorpe, P. Nordlander, S. A. Maier, *Nano Lett.* **2009**, *9*, 1663.
[5] W. Zhou, D. Zhao, Y. C. Shuai, H. Yang, S. Chuwongin, A. Chadha, J. H. Seo, K. X. Wang, V. Liu, Z. Ma, S. Fan, *Prog. Quantum Electron.* **2014**, *38*, 1.
[6] K. L. Lee, J.-B. Huang, J. W. Chang, S. H. Wu, P. K. Wei, *Sci. Rep.* **2015**, *5*, 8547.
[7] L. Stern, M. Grajower, U. Levy, *Nat. Commun.* **2014**, *5*, 4865.
[8] C. Ma, J. Yan, Y. Huang, G. Yang, *Small* **2019**, *15*, 1900546.
[9] P. Pitchappa, A. Kumar, S. Prakash, H. Jani, T. Venkatesan, R. Singh, *Adv. Mater.* **2019**, *31*, 1808157.
[10] T. D. Gupta, L. Martin-Monier, W. Yan, A. L. Bris, T. N. Dang, A. G. Page, K. T. Ho, F. Yesilköy, H. Altug, Y. Qu, F. Sorin, *Nat. Nanotechnol.* **2019**, *14*, 320.
[11] S. C. An, E. Lee, C. H. Lee, H. Y. Jeong, T. S. Kwon, J. H. Lee, Y. C. Jun, *Adv. Opt. Mater.* **2018**, *7*, 1801206.
[12] K. P. Heeg, C. Ott, D. Schumacher, H. C. Wille, R. Röhlsberger, T. Pfeifer, J. Evers, *Phys. Rev. Lett.* **2015**, *114*, 207401.
[13] J. Chen, Z. Li, S. Yue, J. Xiao, Q. Gong, *Nano Lett.* **2012**, *12*, 2494.
[14] C. Wu, A. B. Khanikaev, R. Adato, N. Arju, A. A. Yanik, H. Altug, G. Shvets, *Nat. Mater.* **2012**, *11*, 69.
[15] G. Cao, H. Li, S. Zhan, Z. He, Z. Guo, X. Xu, H. Yang, *Opt. Lett.* **2014**, *39*, 216.
[16] D. L. Sounas, J. Soric, A. Alù, *Nat. Electron.* **2018**, *1*, 113.
[17] W. Ding, B. Luk'yanchuk, C.-W. Qiu, *Phys. Rev. A* **2012**, *85*, 025806.
[18] Z. Chai, X. Hu, H. Yang, Q. Gong, *Nanophotonics* **2017**, *6*, 329.
[19] L. Fan, J. Wang, L. T. Varghese, H. Shen, B. Niu, Y. Xuan, A. M. Weiner, M. Qi, *Science* **2012**, *335*, 447.
[20] B. Peng, Ş. K. Özdemir, F. Lei, F. Monifi, M. Gianfreda, G. L. Long, S. Fan, F. Nori, C. M. Bender, L. Yang, *Nat. Phys.* **2014**, *10*, 394.
[21] Y. Shi, Z. Yu, S. Fan, *Nat. Photonics* **2015**, *9*, 388.
[22] X. Piao, S. Yu, N. Park, *Opt. Express* **2012**, *20*, 18994.
[23] S. K. Ray, A. K. Singh, Ajmal, S. Chandel, P. Mitra, N. Ghosh, *Phys. Rev. A* **2019**, *100*, 033805.
[24] Y. Zhu, X. Hu, Y. Huang, H. Yang, Q. Gong, *Adv. Opt. Mater.* **2013**, *1*, 61.
[25] L. Tao, A. Anopchenko, S. Gurung, J. Zhang, H. W. H. Lee, *Sci. Rep.* **2019**, *9*, 2789.
[26] S. Hayashi, D. V. Nesterenko, A. Rahmouni, Z. Sekkat, *Phys. Rev. B* **2017**, *95*, 165402.
[27] X. Yang, X. Hu, H. Yang, Q. Gong, *Nanophotonics* **2017**, *6*, 365.
[28] J. Xie, X. Niu, X. Hu, F. Wang, Z. Chai, H. Yang, Q. Gong, *Nanophotonics* **2017**, *6*, 1161.
[29] M. Manjappa, P. Pitchappa, N. Singh, N. Wang, N. I. Zheludev, C. Lee, R. Singh, *Nat. Commun.* **2018**, *9*, 4056.
[30] T. Baba, *Nat. Photonics* **2008**, *2*, 465.
[31] M. F. Yanik, W. Suh, Z. Wang, S. Fan, *Phys. Rev. Lett.* **2004**, *93*, 233903.
[32] Z. He, J. Zhao, H. Lu, *Appl. Phys. Express* **2020**, *13*, 012009.
[33] K. Totsuka, N. Kobayashi, M. Tomita, *Phys. Rev. Lett.* **2007**, *98*, 213904.
[34] Q. Xu, P. Dong, M. Lipson, *Nat. Phys.* **2007**, *3*, 406.
[35] A. H. Safavi-Naeini, T. P. M. Alegre, J. Chan, M. Eichenfield, M. Winger, Q. Lin, J. T. Hill, D. E. Chang, O. Painter, *Nature* **2011**, *472*, 69.
[36] J. Chen, K. He, C. Sun, Y. Wang, H. Li, Q. H. Gong, *Opt. Lett.* **2016**, *41*, 2145.
[37] A. Li, W. Bogaerts, *Laser Photonics Rev.* **2019**, *13*, 1800244.
[38] F. Vollmer, L. Yang, *Nanophotonics* **2012**, *1*, 267.
[39] Y. F. Xiao, V. Gaddam, L. Yang, *Opt. Express* **2008**, *16*, 12538.
[40] N. S. King, L. Liu, X. Yang, B. Cerjan, H. O. Everitt, P. Nordlander, N. J. Halas, *ACS Nano* **2015**, *9*, 10628.
[41] F. Hao, P. Nordlander, Y. Sonnefraud, P. V. Dorpe, S. A. Maier, *ACS Nano* **2009**, *3*, 643.
[42] H. D. Deng, X. Y. Chen, Y. Xu, A. E. Miroshnichenko, *Nanoscale* **2015**, *7*, 20405.
[43] Y. Zhang, Y. R. Zhen, O. Neumann, J. K. Day, P. Nordlander, N. J. Halas, *Nat. Commun.* **2014**, *5*, 4424.
[44] D. Bekele, Y. Yu, K. Yvind, J. Mork, *Laser Photonics Rev.* **2019**, *13*, 1900054.
[45] Y. Xu, A. E. Miroshnichenko, *Phys. Rev. B* **2014**, *89*, 134306.
[46] Y. Hua, A. K. Fumani, T. W. Odom, *ACS Photonics* **2019**, *6*, 322.
[47] K. L. Lee, M. L. You, X. Shi, Y. R. Li, K. Ueno, H. Misawa, P. K. Wei, *Appl. Mater. Today* **2019**, *16*, 72.
[48] D. L. Sounas, A. Alù, *Phys. Rev. B* **2018**, *97*, 115431.
[49] S. H. Wu, K. L. Lee, A. Chiou, X. Cheng, P. K. Wei, *Small* **2013**, *9*, 3532.
[50] W. X. Lim, M. Manjappa, Y. K. Srivastava, L. Cong, A. Kumar, K. F. MacDonald, R. Singh, *Adv. Mater.* **2018**, *30*, 1705331.
[51] M. Manjappa, Y. K. Srivastava, L. Cong, I. Al-Naib, R. Singh, *Adv. Mater.* **2017**, *29*, 1603355.
[52] N. Liu, T. Weiss, M. Mesch, L. Langguth, U. Eigenthaler, M. Hirscher, C. Sönnichsen, H. Giessen, *Nano Lett.* **2010**, *10*, 1103.
[53] N. Papasimakis, N. I. Zheludev, *Opt. Photonics News* **2009**, *20*, 22.
[54] C. Yan, K. Y. Yang, O. J. F. Martin, *Light: Sci. Appl.* **2017**, *6*, 17017.
[55] H. X. Xu, G. Hu, Y. Li, L. Han, J. Zhao, Y. Sun, F. Yuan, G. M. Wang, Z. H. Jiang, X. Ling, T. J. Cui, C.-W. Qiu, *Light: Sci. Appl.* **2019**, *8*, 3.
[56] C.-W. Qiu, S. Zhang, F. Capasso, Y. Kivshar, *ACS Photonics* **2018**, *5*, 1640.
[57] S. H. Mousavi, A. B. Khanikaev, J. Allen, M. Allen, G. Shvets, *Phys. Rev. Lett.* **2014**, *112*, 117402.
[58] L. Fan, L. T. Varghese, J. Wang, Y. Xuan, A. M. Weiner, M. Qi, *Opt. Lett.* **2013**, *38*, 1259.
[59] M. Eitan, Z. Iluz, Y. Yifat, A. Boag, Y. Hanein, J. Scheuer, *ACS Photonics* **2015**, *2*, 615.
[60] Y. Huang, C. Min, P. Dastmalchi, G. Veronis, *Opt. Express* **2015**, *23*, 14922.
[61] A. A. Yanik, M. Huang, O. Kamohara, A. Artar, T. W. Geisbert, J. H. Connor, H. Altug, *Nano Lett.* **2010**, *10*, 4962.
[62] Y. Deng, G. Cao, H. Yang, X. Zhou, Y. Wu, *Plasmonics* **2018**, *13*, 345.
[63] G. Cao, H. Li, Y. Deng, S. Zhan, Z. He, B. Li, *Opt. Express* **2014**, *22*, 25215.
[64] H. Yang, G. Cao, X. Shang, T. Li, G. Yang, G. Li, *J. Phys. D: Appl. Phys.* **2019**, *53*, 045104.
[65] X. Huang, X. Feng, L. Chen, L. Wang, W. C. Tan, L. Huang, K. W. Ang, *Nano Energy* **2019**, *62*, 667.
[66] L. M. Zhou, K. W. Xiao, J. Chen, N. Zhao, *Laser Photonics Rev.* **2017**, *11*, 1600284.
[67] X. Zhang, Q. Cao, Z. Wang, Y. Liu, C. Qiu, L. Yang, Q. Gong, Y. Xiao, *Nat. Photonics* **2019**, *13*, 21.
[68] M. Qiu, W. Ren, T. Jeong, M. Won, G. Y. Park, D. K. Sang, L. Liu, H. Zhang, J. S. Kim, *Chem. Soc. Rev.* **2018**, *47*, 5588.
[69] T. Wang, D. Qi, H. Yang, Z. Liu, M. Wang, W. R. Leow, G. Chen, J. Yu, K. He, H. Cheng, Y. Wu, H. Zhang, X. Chen, *Adv. Mater.* **2019**, *31*, 1803883.

[70] G. Hu, X. Hong, K. Wang, J. Wu, H. Xu, W. Zhao, W. Liu, S. Zhang, F. Garcia Vidal, B. Wang, P. Lu, C.-W. Qiu, *Nat. Photonics* **2019**, *13*, 467.
[71] G. Hu, J. Shen, C.-W. Qiu, A. Alù, S. Dai, *Adv. Opt. Mater.* **2019**, *8*, 1901393.
[72] R. Zhou, J. Peng, S. Yang, D. Liu, Y. Xiao, G. Cao, *Nanoscale* **2018**, *10*, 18878.
[73] W. Cao, R. Singh, C. Zhang, J. Han, M. Tonouchi, W. Zhang, *Appl. Phys. Lett.* **2013**, *103*, 101106.
[74] Y. K. Srivastava, M. Manjappa, L. Cong, H. N. S. Krishnamoorthy, V. Savinov, P. Pitchappa, R. Singh, *Adv. Mater.* **2018**, *30*, 1801257.
[75] Z. Shen, S. Zhou, S. Ge, W. Hu, Y. Lu, *Appl. Phys. Lett.* **2019**, *114*, 041106.
[76] A. H. Gevorgyan, *Phys. Rev. E* **2019**, *99*, 012702.
[77] J. Chen, P. Wang, H. Ming, J. R. Lakowicz, D. Zhang, *Phys. Rev. B* **2019**, *99*, 115420.
[78] C. Cui, C. Zhou, S. Yuan, X. Qiu, L. Zhu, Y. Wang, Y. Li, J. Song, Q. Huang, Y. Wang, C. Zeng, J. Xia, *ACS Photonics* **2018**, *5*, 4074.
[79] Y. Moritake, Y. Kanamori, K. Hane, *Sci. Rep.* **2016**, *6*, 33208.
[80] M. I. Stockman, *Nat. Photonics* **2008**, *2*, 327.
[81] K. Tanaka, E. Plum, J. Y. Ou, T. Uchino, N. I. Zheludev, *Phys. Rev. Lett.* **2010**, *105*, 227403.
[82] T. S. Rasmussen, Y. Yu, J. Mork, *Laser Photonics Rev.* **2017**, *11*, 1700089.
[83] M. F. Limonov, M. V. Rybin, A. N. Poddubny, Y. S. Kivshar, *Nat. Photonics* **2017**, *11*, 543.
[84] G. Haran, L. Chuntonov, *Chem. Rev.* **2018**, *118*, 5539.
[85] W. X. Lim, M. Manjappa, P. Pitchappa, R. Singh, *Adv. Opt. Mater.* **2018**, *6*, 1800502.
[86] J. Chen, F. Gan, Y. Wang, G. Li, *Adv. Opt. Mater.* **2018**, *6*, 1701152.
[87] X. Niu, X. Hu, Q. Yan, J. Zhu, H. Cheng, Y. Huang, C. Lu, Y. Fu, Q. Gong, *Nanophotonics* **2019**, *8*, 1125.
[88] Z. Chai, X. Hu, C. Li, H. Yang, Q. Gong, *ACS Photonics* **2016**, *3*, 2068.
[89] G. Cao, H. Li, S. Zhan, H, Xu , Z. Liu, Z. He, Y. Wang, *Opt. Express* **2013**, *21*, 9198.
[90] Y. Deng, G. Cao, H. Yang, G. Li, X. Chen, W. Lu, *Sci. Rep.* **2017**, *7*, 10639.
[91] Y. Deng, G. Cao, H. Yang, *Photonics Nanostruct.* **2018**, *28*, 45.
[92] F. Xia, L. Sekaric, Y. Vlasov, *Nat. Photonics* **2007**, *1*, 65.
[93] Y. Huang, C. Min, G. Veronis, *Appl. Phys. Lett.* **2011**, *99*, 143117.
[94] Y. P. Rakovich, J. F. Donegan, *Laser Photonics Rev.* **2010**, *4*, 179.
[95] M. Bayer, T. Gutbrod, J. P. Reithmaier, A. Forchel, T. L. Reinecke, P. A. Knipp, A. A. Dremin, V. D. Kulakovskii, *Phys. Rev. Lett.* **1998**, *81*, 2582.
[96] M. Menotti, B. Morrison, K. Tan, Z. Vernon, J. E. Sipe, M. Liscidini, *Phys. Rev. Lett.* **2019**, *122*, 013904.
[97] M. Zhang, C. Wang, Y. Hu, A. Shams-Ansari, T. Ren, S. Fan, M. Lončar, *Nat. Photonics* **2019**, *13*, 36.
[98] D. Venkatakrishnarao, E. A. Mamonov, T. V. Murzina, R. Chandrasekar, *Adv. Opt. Mater.* **2018**, *6*, 1800343.
[99] T. Siegle, S. Schierle, S. Kraemmer, B. Richter, S. F. Wondimu, P. Schuch, C. Koos, H. Kalt, *Light: Sci. Appl.* **2017**, *6*, 16224.
[100] J. Wang, Y. Yin, Q. Hao, Y. Zhang, L. Ma, O. G. Schmidt, *Adv. Opt. Mater.* **2018**, *6*, 1700842.
[101] Y. Li, F. Abolmaali, K. W. Allen, N. I. Limberopoulos, A. Urbas, Y. Rakovich, A. V. Maslov, V. N. Astratov, *Laser Photonics Rev.* **2017**, *11*, 1600278.
[102] Y. Yang, I. I. Kravchenko, D. P. Briggs, J. Valentine, *Nat. Commun.* **2014**, *5*, 5753.
[103] S. Fan, W. Suh, J. D. Joannopoulos, *J. Opt. Soc. Am. A* **2003**, *20*, 569.
[104] H. A. Haus, W. Huang, *Proc. IEEE* **1991**, *79*, 1505.
[105] Y. F. Xiao, M. Li, Y. C. Liu, Y. Li, X. Sun, Q. Gong, *Phys. Rev. A* **2010**, *82*, 065804.
[106] Q. Li, T. Wang, Y. Su, M. Yan, M. Qiu, *Opt. Express* **2010**, *18*, 8367.
[107] W. Suh, Z. Wang, S. Fan, *IEEE J. Quantum Electron* **2004**, *40*, 1511.
[108] X. Tu, L. Y. Mario, T. Mei, *Opt. Express* **2010**, *18*, 18820.
[109] S. Fan, *Appl. Phys. Lett.* **2002**, *80*, 908.
[110] H. A. Haus, Y. Y. Lai, *J. Lightwave Technol.* **1991**, *9*, 754.
[111] Y. F. Xiao, L. He, J. Zhu, L. Yang, *Appl. Phys. Lett.* **2009**, *94*, 231115.
[112] B. B. Li, Y. F. Xiao, C. L. Zou, Y. C. Liu, X. F. Jiang, Y. L. Chen, Y. Li, Q. Gong, *Appl. Phys. Lett.* **2011**, *98*, 021116.
[113] U. Fano, *II Nuovo Cimento* **1935**, *129*, 154.
[114] Y. C. Liu, B. B. Li, Y. F. Xiao, *Nanophotonics* **2017**, *6*, 789.
[115] Y. Yu, H. Hu, L. K. Oxenløwe, K. Yvind, J. Mork, *Opt. Lett.* **2015**, *40*, 2357.
[116] S. Han, L. Cong, Y. K. Srivastava, B. Qiang, M. V. Rybin, A. Kumar, R. Jain, W. X. Lim, V. G. Achanta, S. S. Prabhu, Q. J. Wang, Y. S. Kivshar, R. Singh, *Adv. Mater.* **2019**, *31*, 1901921.
[117] C. Zhou, G. Liu, G. Ban, S. Li, Q. Huang, J. Xia, Y. Wang. M. Zhan, *Appl. Phys. Lett.* **2018**, *112*, 101904.
[118] X. Tian, Z. Liu, H. Lin, B. Jia, Z.-Y. Li, J. Li, *Nanoscale* **2018**, *10*, 16630.
[119] P. Tassin, L. Zhang, R. Zhao, A. Jain, T. Koschny, C. M. Soukoulis, *Phys. Rev. Lett.* **2012**, *109*, 187401.
[120] Z. He, H. Li, S. Zhan, G. Cao, B. Li, *Opt. Lett.* **2014**, *39*, 5543.
[121] Z. He, H. Li, S. Zhan, B. Li, Z. Chen, H. Xu, *IEEE Photonics Technol. Lett.* **2015**, *27*, 2371.
[122] Z. He, Y. P, B. Li, Z Chen, H. Xu, M. Zheng, H. Li, *Appl. Phys. Express* **2016**, *9*, 072002.
[123] Z. He, H. Li, S. Zhan, B. Li, Z. Chen, H. Xu, *Sci. Rep.* **2015**, *5*, 15837.
[124] S. Yuan, L. Chen, Z. Wang, R. Wang, X. Wu, X. Zhang, *Appl. Phys. Lett.* **2019**, *115*, 201102.
[125] M. A. Miri, A. Alù, *Science* **2019**, *363*, eaar7709.
[126] Z. Dong, Z. Li, F. Yang, C.-W. Qiu, J. S. Ho, *Nat. Electronics* **2019**, *2*, 335.
[127] W. Chen, Ş. K. Özdemir, G. Zhao, J. Wiersig, L. Yang, *Nature* **2017**, *548*, 192.
[128] J. Zhu, S. K. Ozdemir, Y.-F. Xiao, L. Li, L. He, D. R. Chen, L. Yang, *Nat. Photonics* **2010**, *4*, 46.
[129] L. He, Ş. K. Özdemir, J. Zhu, W. Kim, L. Yang, *Nat. Nanotechnol.* **2011**, *6*, 428.
[130] K. D. Heylman, N. Thakkar, E. H. Horak, S. C. Quillin, C. Cherqui, K. A. Knapper, D. J. Masiello, R. H. Goldsmith, *Nat. Photonics* **2016**, *10*, 788.
[131] B. Min, L. Yang, K. Vahala, *Phys. Rev. A* **2007**, *76*, 013823.
[132] Y. F. Xiao, X. F. Jiang, Q. F. Yang, L. Wang, K. Shi, Y. Li, Q. Gong, *Laser Photonics Rev.* **2013**, *7*, L51.
[133] M. Ono, M. Hata, M. Tsunekawa, K. Nozaki, H. Sumikura, H. Chiba, M. Notomi, *Nat. Photonics* **2020**, *14*, 37.
[134] J. Chen, C. Sun, Q. Gong, *Opt. Lett.* **2014**, *39*, 52.
[135] Z. He, H. Li, B. Li, Z. Chen, H. Xu, M. Zheng, *Opt. Lett.* **2016**, *41*, 5206.
[136] G. Lin, H. Yang, Y. Deng, D. Wu, X. Zhou, Y. Wu, G. Cao, J. Chen, W. Sun, R. Zhou, *Opt. Express* **2019**, *27*, 33359.
[137] Z. Chai, X. Hu, Y. Zhu, S. Sun, H. Yang, Q. Gong, *Adv. Opt. Mater.* **2014**, *2*, 320.
[138] Y. Yu, Y. Chen, H. Hu, W. Xue, K. Yvind, J. Mork, *Laser Photonics Rev.* **2015**, *9*, 241.
[139] M. Heuck, P. T. Kristensen, Y. Elesin, J. Mørk, *Opt. Lett.* **2013**, *38*, 2466.
[140] Y. L. Shang, M. Y. Ye, X. M. Lin, *Photonics Res.* **2017**, *5*, 119.
[141] L. Gu, H. Fang, J. Li, L. Fang, S. J. Chua, J. Zhao, X. Gan, *Nanophotonics* **2019**, *8*, 841.
[142] Q. Xu, S. Sandhu, M. L. Povinelli, J. Shakya, S. Fan, M. Lipson, *Phys. Rev. Lett.* **2006**, *96*, 123901.
[143] Z. Han, S. I. Bozhevolnyi, *Opt. Express* **2011**, *19*, 3251.

[144] H. Lu, X. Liu, D. Mao, G. Wang, *Opt. Lett.* **2012**, *37*, 3780.
[145] C. Xiong, H. Li, H. Xu, M. Zhao, B. Zhang, C. Liu, K. Wu, *Opt. Express* **2019**, *27*, 17718.
[146] S. Li, Y. Wang, R. Jiao, L. Wang, G. Duan, L. Yu, *Opt. Express* **2017**, *25*, 3525.
[147] X. F. Liu, F. Lei, M. Gao, X. Yang, C. Wang, Ş. K. Özdemir, L. Yang, G. L. Long, *Opt. Express* **2016**, *24*, 9550.
[148] Z. Tu, D. Gao, M. Zhang, D. Zhang, *Opt. Lett.* **2017**, *25*, 20911.
[149] Z. Chai, Y. Zhu, X. Hu, X. Yang, Z. Gong, F. Wang, H. Yang, Q. Gong, *Adv. Opt. Mater.* **2016**, *4*, 1159.
[150] N. Caselli, F. Intonti, F. L. China, F. Biccari, F. Riboli, A. Gerardino, L. Li, E. H. Linfield, F. Pagliano, A. Fiore, M. Gurioli, *Nat. Commun.* **2018**, *9*, 396.
[151] X. Yang, M. Yu, D.-L. Kwong, C. W. Wong, *Phys. Rev. Lett.* **2009**, *102*, 173902.
[152] C. Yang, X. Jiang, Q. Hua, S. Hua, Y. Chen, J. Ma, M. Xiao, *Laser Photonics Rev.* **2017**, *11*, 1600178.
[153] B. B. Li, Y. F. Xiao, C. L. Zou, X. F. Jiang, Y. C. Liu, F. W. Sun, Y. Li, Q. Gong, *Appl. Phys. Lett.* **2012**, *100*, 021108.
[154] C. Yang, Y. Hu, X. Jiang, M. Xiao, *Phys. Rev. A* **2017**, *95*, 033847.
[155] Ş. K. Özdemir, S. Rotter, F. Nori, L. Yang, *Nat. Mater.* **2019**, *18*, 783.
[156] Y. Li, Y. G. Peng, L. Han, M. A. Miri, W. Li, M. Xiao, X. F. Zhu, J. Zhao, A. Alù, S. Fan, C.-W. Qiu, *Science* **2019**, *364*, 170.
[157] C. E. Rüter, K. G. Makris, R. El-Ganainy, D. N. Christodoulides, M. Segev, D. Kip, *Nat. Phys.* **2010**, *6*, 192.
[158] A. Regensburger, C. Bersch, M.-A. Miri, G. Onishchukov, D. N. Christodoulides, U. Peschel, *Nature* **2012**, *488*, 167.
[159] J. Li, R. Yu, C. Ding, Y. Wu, *Phys. Rev. A* **2016**, *93*, 023814.
[160] J. Li, R. Yu, Y. Wu, *Phys. Rev. A* **2016**, *94*, 063822.
[161] H. Lu, X. Liu, D. Mao, *Phys. Rev. A* **2012**, *85*, 053803.
[162] J. Chen, C. Wang, R. Zhang, J. Xiao, *Opt. Lett.* **2012**, *37*, 5133.
[163] Y. Liu, S. Zhan, G. Cao, J. Li, H. Yang, Q. Liu, S. Hu, G. Nie, Y. Gao, X. Wu, *IEEE J. Quantum Electron.* **2019**, *25*, 4600206.
[164] Z. Chai, X. Hu, F. Wang, X. Niu, J. Xie, Q. Gong, *Adv. Opt. Mater.* **2017**, *5*, 1600665.
[165] J. Chen, Z. Li, X. Zhang, J. Xiao, Q. Gong, *Sci. Rep.* **2013**, *3*, 1451.
[166] S. Zhang, J. Zhou, Y. S. Park, J. Rho, R. Singh, S. Nam, A. K. Azad, H. T. Chen, X. Yin, A. J. Taylor, X. Zhang, *Nat. Commun.* **2012**, *3*, 942.
[167] K. F. MacDonald, Z. L. Sámson, M. I. Stockman, N. I. Zheludev, *Nat. Photonics* **2009**, *3*, 55.
[168] X. Zhang, B. Sun, J. M. Hodgkiss, R. H. Friend, *Adv. Mater.* **2008**, *20*, 4455.
[169] G. A. Wurtz, R. Pollard, A. V. Zayats, *Phys. Rev. Lett.* **2006**, *97*, 057402.
[170] K. Nozaki, A. Shinya, S. Matsuo, T. Sato, E. Kuramochi, M. Notomi, *Opt. Express* **2013**, *21*, 11877.
[171] L. Bi, J. Hu, P. Jiang, D. H. Kim, G. F. Dionne, L. C. Kimerling, C. A. Ross, *Nat. Photonics* **2011**, *5*, 758.
[172] M. Tamagnone, A. Fallahi, J. R. Mosig, J. Perruisseau-Carrier, *Nat. Photonics* **2014**, *8*, 556.
[173] X. Hu, Z. Li, J. Zhang, H. Yang, Q. Gong, X. Zhang, *Adv. Funct. Mater.* **2011**, *21*, 1803.
[174] C. Fan, F. Shi, H. Wu, Y. Chen, *Opt. Lett.* **2015**, *40*, 2449.
[175] R. M. Ma, R. F. Oulton, *Nat. Nanotechnol.* **2019**, *14*, 12.
[176] R. M. Ma, *Nat. Mater.* **2019**, *18*, 1152.
[177] R. B. Wu, Y. Zheng, Q. M. Chen, Y. Liu, *Phys. Rev.* **2018**, *98*, 033817.
[178] A. Dutt, Q. Lin, L. Yuan, M. Minkov, M. Xiao, S. Fan, *Science* **2020**, *367*, 59.
[179] T. Ozawa, H. M. Price, *Nat. Rev. Phys.* **2019**, *1*, 349.
[180] F. Zangeneh-Nejad, R. Fleury, *Phys. Rev. Lett.* **2019**, *122*, 014301.